Journal of Power Sources 196 (2011) 7257–7262

Contents lists available at ScienceDirect

Journal of Power Sources

journal homepage: www.elsevier.com/locate/jpowsour

Performance analysis of mixed ionic–electronic conducting cathodes in anode supported cells

Cornelia Endler-Schuck[a,*], André Leonide[a], André Weber[a], Sven Uhlenbruck[b], Frank Tietz[b], Ellen Ivers-Tiffée[a]

[a] Karlsruher Institut für Technologie (KIT), Institut für Werkstoffe der Elektrotechnik (IWE), Adenauerring 20b, D-76131 Karlsruhe, Germany
[b] Institut für Energieforschung (IEF-1), Forschungszentrum Jülich, D-52425 Jülich, Germany

ARTICLE INFO

Article history:
Received 28 June 2010
Received in revised form
17 November 2010
Accepted 17 November 2010
Available online 25 November 2010

Keywords:
LSCF
Degradation behaviour
Equivalent circuit model

ABSTRACT

The analysis of mixed ionic–electronic conducting (MIEC) cathodes with respect to operation temperature and time is essential for a target-oriented development of anode-supported solid oxide fuel cells (ASCs). This study tracks both issues by impedance spectroscopy on a high-performance cathode with the composition $La_{0.58}Sr_{0.4}Co_{0.2}Fe_{0.8}O_{3-\delta}$ (LSCF).

A wide set of impedance spectra were sampled at 600, 750 and 900 °C over the entire operation time of 1000 h. The identification and quantification of the individual anodic and cathodic contributions to the polarization losses of an ASC were enabled by an appropriate equivalent circuit model. For this purpose, the impedance data sets were evaluated subsequently by (i) a DRT (distribution of relaxation times) analysis followed by (ii) a CNLS fit. The cathodic polarization resistance is attributed to the oxygen surface exchange and the bulk diffusion of oxygen ions and is described by a Gerischer element.

The anodic polarization resistance is described by a Warburg element and two RQ elements according to physical origins. The thorough analysis of all data sets leads to the surprising outcome that the cathode degradation is most pronounced and moreover, increases with decreasing temperature. After 1000 h of operation, the cathode polarization resistance raised steeply from 0.012%/h at 900 °C over 0.28%/h at 750 °C to 1.49%/h at 600 °C. These latest findings will have far-reaching implications for the development of MIEC cathodes.

1. Introduction

$La_{0.58}Sr_{0.4}Co_{0.2}Fe_{0.8}O_{3-\delta}$ (LSCF) as a mixed ionic and electronic conductor (MIEC) was reported as one of the best performing cathode materials for intermediate-temperature solid oxide fuel cells (IT-SOFC). Preliminary parameter studies concluded that the degradation rate for anode supported cells (ASCs) with composite LSM–YSZ cathode is smaller ($\Delta V/V$ = 0.5%/1000 h at 800 °C) [1] compared to LSCF cathodes ($\Delta V/V$ = 0.9–1.5%/1000 h at 800 °C [2–4].

Our long term study focuses on the LSCF cathode degradation course in a state-of-the-art ASC at temperatures of 600, 750 and 900 °C. This range represents the customary temperature load of mobile (600–800 °C) and small stationary (700–900 °C) SOFC power systems. As reference electrodes are not applicable, the contributions of ohmic and polarization losses of electrolyte, anode and cathode have to be identified by high resolution impedance studies based on a combination of DRT (distribution of relaxation times) analysis followed by a complex nonlinear least square (CNLS) fitting approach. This approach, in combination with a recently developed equivalent circuit model, opened new perspectives for a detailed examination of polarization losses in ASC [5]. Based on these results, we already separated and quantified the individual polarization processes of anode substrate, anode functional layer and cathode in a former long term study at T = 750 °C for t = 700 h [6]. As a result the increase in cathode resistance determines the degradation behaviour of the cell but the anode polarization resistance (both substrate and functional layer) is still responsible for the main part of the cell losses. This extensive study provided a reliable basis to differentiate the time and temperature dependant cathode and anode polarization resistances over a wide temperature range, which is discussed in the present paper. Accordingly, the present state of knowledge about the temperature dependent degradation behaviour is inconsistent: ASCs with LSCF cathode show a more pronounced degradation at T = 800 °C when compared to T = 700 °C [1] indicating a temperature driven degradation mechanism. ASCs with LSM–YSZ cathode show a reversal tendency: the degradation increases with decreasing temperature [7].

* Corresponding author. Tel.: +49 721 60848148; fax: +49 721 60847492.
E-mail addresses: Cornelia.Endler@kit.edu, endler@kit.edu (C. Endler-Schuck).

0378-7753/$ – see front matter © 2010 Elsevier B.V. All rights reserved.
doi:10.1016/j.jpowsour.2010.11.079

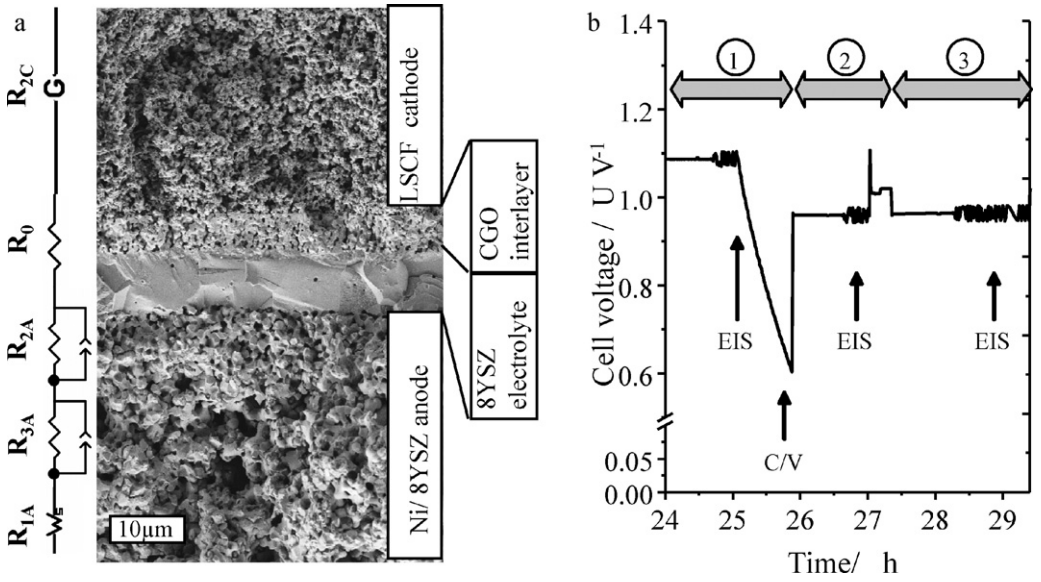

Fig. 1. (a) A scanning electron micrograph of the cross-section of a fractured cell showing part of the porous anode and cathode, the dense electrolyte, and the CGO interlayer. On the left hand side the equivalent circuit diagram for this type of cell is shown. It was used for separating the losses of electrolyte, anode and cathode consisting of (i) ohmic resistance R_0, (ii) 2 serial RQ elements (R_{2A} and R_{3A}), (iii) a Gerischer element (R_{2C}), (iv) and a generalized finite length Warburg element (G-FLW) (R_{1A}). (b) Measurement procedure with air at the cathode and (1) H_2–H_2O (95/5), (2) H_2–H_2O (40/60) and (3) CO–CO_2 (50/50) at the anode sequentially carried out each 8 h (0–300 h) and 14 h (300–1000 h). Electrochemical impedance measurements (EIS) and *C*/*V* curves were carried out as indicated at each gas composition. At T = 600 °C the (3) CO–CO_2 (50/50) gas composition was not supplied to the anode to avoid carbon formation.

In this study the temperature dependent degradation course of ASCs with LSCF cathode and screen printed GCO interlayer is analysed more systematically. The time-related change of the ASC performance was recorded every 10 h by impedance measurements in a frequency range from 10 mHz to 1 MHz, altogether for more than 1000 h of operation at T = 600 °C, 750 °C and 900 °C. The anodic and cathodic polarization resistance was identified by well selected and adapted experimental parameters. All experiments reported here were conducted under open-circuit conditions (OCV) as former long term studies of identical ASCs [3,8] showed no difference between degradation rates evaluated for OCV, 300 and 600 mA/cm^2.

2. Experiments

2.1. Cell characteristics

The single cells used in this study are based on 50 mm × 50 mm anode substrates (Ni/8 mol% yttria doped zirconia (8YSZ)) with an average thickness of about 1 mm. On these substrates, an "anode functional layer (AFL)" (Ni/8YSZ, approximately 10 μm), and an electrolyte (8YSZ, approximately 10 μm), were deposited and co-fired at T = 1400 °C. A $Ce_{0.8}Gd_{0.2}O_{2-\delta}$ (CGO, from Treibacher Auermet, Austria) interlayer was screen-printed on the electrolyte and sintered at T = 1300 °C for t = 3 h, resulting in a thickness of approximately 7 μm [4]. This interlayer was used to prevent a chemical reaction between LSCF and 8YSZ, which otherwise forms an insulating layer of $SrZrO_3$. On top of this interlayer, a $La_{0.58}Sr_{0.4}Co_{0.2}Fe_{0.8}O_{3-\delta}$ cathode was applied by screen-printing, resulting in a thickness of approximately 45 μm after sintering. Details regarding the manufacturing procedures can be found elsewhere [4,9]. The active area of the working cathode was 10 mm × 10 mm. Two auxiliary electrodes in gas flow direction in front and behind the cathode were applied for OCV control. In Fig. 1(a)), a scanning electron micrograph of the cross-section of a fractured cell shows a part of the porous anode, the dense electrolyte, the CGO interlayer, and a part of the porous cathode.

The ASC was inserted into an Al_2O_3 housing, which was located in the high temperature part of the measurement setup. More information about electrical contacts and sealing can be found elsewhere [10]. The appropriate fuel gas flow and composition was computer controlled by digital mass flow controllers (MFCs). On the cathode side, one MFC is available for air supply. On the anode side, four gases (H_2, O_2, CO and CO_2) are provided to compose the different gas compositions. Fig 1(b) shows a part of the measurement procedure which is sequentially carried out, each 8 h at t = 0–270 h and each 14 h at t = 270–1000 h. Within this part, the gas composition at the anode changed three times [(1) H_2–H_2O (95/5), (2) H_2–H_2O (40/60), and (3) CO–CO_2 (50/50)], while the cathode gas composition was kept constant with 250 mL/min air during the entire measurement. This measurement procedure is used for the long term measurements at T = 750 and 900 °C. The change from H_2–H_2O to a CO–CO_2 gas mixture proved to be crucial for the separation and deconvolution of the P_{1A} and P_{2C} contributions (the processes P_{1A} and P_{2C} are explained in Section 2.2). The CO–CO_2 gas mixture has a lower binary diffusion coefficient compared to H_2–H_2O. A shift in the relaxation time to lower frequencies corresponds to a decrease in the gas diffusion coefficient and to an increase in the gas diffusion resistance in the anode microstructure. At T = 600 °C the CO–CO_2 (50/50) gas composition was not supplied at the anode to avoid carbon formation. Impedance measurements were carried out with a Solartron 1260 frequency response analyzer in a frequency range from 10 mHz to 1 MHz. Due to the fact that the current density had no obvious impact on the cell degradation in former long-term measurements [3], all experiments were conducted under OCV. During the gas composition, (1) H_2–H_2O (95/5) a current–voltage (*C*/*V*) curve was measured after each impedance spectrum. Table 1 shows the sample ID, measurement time and temperature as well as the gas composition at cathode and anode side.

2.2. Equivalent circuit analysis

The CNLS fit of the impedance data was carried out with the commercially available software Z-View® [11]. The applied equiv-

Table 1
Anode supported cells measured in long term measurements for this study.

Sample	$T_{measurement}$	$t_{measurement}$	Cathode gas composition	Anode gas composition
Cell A	600 °C	1030 h	Air	(1) H_2–H_2O (95/5), (2) H_2–H_2O (40/60),
Cell B	750 °C	1012 h	Air	(1) H_2–H_2O (95/5), (2) H_2–H_2O (40/60), (3) CO–CO_2 (50/50)
Cell C	900 °C	1033 h	Air	(1) H_2–H_2O (95/5), (2) H_2–H_2O (40/60), (3) CO–CO_2 (50/50)

alent circuit model was developed by a pre-identification of the impedance response by calculating and analyzing the corresponding DRT and has been presented in [5]. A detailed description of the DRT method and its application is given in [5,12,13]. The equivalent circuit model (see Fig. 1(a)) used in this study consists of four impedance elements connected in series. The anode processes P_{1A}, P_{2A} and P_{3A} are modeled by a generalized finite length Warburg element (G-FWS element) and two RQ elements, whereas the cathode process P_{2C} is modeled by a Gerischer element. Each equivalent circuit element is attributed to a physical process [5]. P_{1A} describes the anode gas diffusion resistance. P_{2A} and P_{3A} can be assigned to the impedance of (i) the lattice network structure of the Ni/8YSZ anode charge transfer reaction at the triple phase boundary, (ii) ionic transport in the Ni/YSZ structure, and (iii) gas diffusion limitation inside the pores of the AFL in approximately the first 100 h of operation [13,14]. The cathode polarization process P_{2C} is related to the cathodic losses originate from oxygen surface exchange kinetics and from the diffusivity of oxygen ions through the LSCF bulk (R_{2C}) [5,15]. The frequency ranges of each polarization process were determined by the DRT method. With these start values the EIS spectra were fitted by a CNLS fit. The resulting detailed temperature and time dependent behavior of the ohmic resistance R_0, the total polarization resistance R_{pol}, each anode contribution R_{1A}, R_{2A} and R_{3A} and the cathode polarization resistance R_{2C} were discussed and shown in the following sections. We describe the polarization processes as P_{1A}, P_{2C}, P_{2A} and P_{3A} and the corresponding polarization resistances or losses as R_{1A}, R_{2C}, R_{2A} and R_{3A} considering the resistance values obtained by the CNLS fit.

3. Results

The time- and temperature dependent behaviour of the total polarization losses R_{pol}, the ohmic resistance R_0, the anode contributions R_{1A}, R_{2A}, R_{3A}, the total anode resistance $R_{anode\ total}$ and the cathode polarization resistance R_{2C} are shown in Fig. 2. The resistances at T = 600 °C are determined in anode gas mixture (2) (H_2–H_2O (40/60)), for T = 750 °C and 900 °C all contributions are determined in anode gas mixture (3) (CO–CO_2 (50/50)). The corresponding values for selected measurements and the calculated degradation rates for R_{pol} and R_{2C} are recorded in Tables 2 and 3.

3.1. Total polarization resistance R_{pol}

The total polarization resistance R_{pol} (see Fig. 2(a)) describes the sum of the polarization losses R_{1A}, R_{2A}, R_{3A} and R_{2C}. The degradation rates per hour are shown in Table 2. R_{pol} decreases with increasing operating temperature (R_{pol} = 1.317 Ω cm^2 at T = 600 °C, 0.207 Ω cm^2 at T = 750 °C and 0.0998 Ω cm^2 at T = 900 °C) due to the thermal activation of the electrochemical electrode processes.

At T = 600 °C the nonlinear degradation curve increases from 1.317 Ω cm^2 to 3.804 Ω cm^2 during the long term measurement. The degradation rate is very small in the first 304 h with 0.049%/h and increases in the second part at t = 304–1033 h with 0.209%/h which can be clearly observed in Fig. 2(a) and Table 2. At T = 750 °C the degradation rate is overall smaller compared to T = 600 °C with 0.012%/h (t = 11–1304 h) and 0.02%/h (t = 304–1012 h). The lowest degradation rates are measured at T = 900 °C during t = 1000 h. Values of -4.1×10^{-3}%/h (t = 3–306 h) and -4.4×10^{-4}%/h (t = 306–1031 h) were determined. These findings give evidence that the degradation of total polarization resistance shows a nonlinear behavior and increases with decreasing temperature.

The degradation behavior found in this study is inconsistent to the findings of Becker [1]. ASCs with LSCF cathode show a higher degradation rate at T = 800 °C compared to T = 700 °C in long term measurements indicating a temperature-driven degradation mechanism. ASCs with LSM/YSZ cathode show a reversal tendency: the cells measured at three different temperatures and different current densities show significant smaller degradations rates at 850 °C (950 °C) than at 750 °C [7]. This behavior is more similar to our observations at 600 °C, 750 °C and 900 °C.

3.2. Ohmic resistance R_0

The ohmic resistance R_0 consists of the ohmic part of the 8YSZ electrolyte and the porous screen-printed CGO interlayer. The ohmic contributions of the LSCF cathode and the Ni/YSZ anode can be neglected, because these material posses electrical conductivities that are several orders of magnitude higher compared to the electrolyte material ($\sigma_{La0.6Sr0.4Co0.2Fe0.8O3-\delta}$ = 290 S/cm at 750 °C [16], $\sigma_{Ni/8YSZ}$ = 10^3 S/cm [17], σ_{8YSZ} = 0.03 S/cm [18]). The theoretical resistance $R_{0,theoretical}$ was calculated from the electrical conductivities and the layer thicknesses. The measured ohmic resistance R_0 of the bilayer YSZ/CGO is four times larger than $R_{0,theoretical}$ = 35 mΩ cm^2. This is mainly caused by the YSZ/CGO interdiffusion at sintering temperatures of T = 1300 °C and a little by the porosity in the CGO interlayer. Furthermore, a minor part is probably caused by a current constriction in the electrolyte at the cathode/CGO interface and at the anode/YSZ interface [6].

The long term behavior of the ohmic resistance R_0 (Fig. 2(b)) has also a temperature dependent characteristic: For T = 600 °C R_0 remains constant (−0.6%/1025 h), while a slight decrease by 4.5%/1012 h can be observed at T = 750 °C. This slight decrease can be attributed to an initial sintering process of the LSCF layer [6]. At T = 900 °C an increase by 17%/1031 h probably indicates a degradation of the bilayer 8YSZ/CGO at T = 900 °C. Müller [17] investigated the intrinsic degradation of 8YSZ electrolytes and found an increase of degradation rate with increasing temperature (T = 860 °C, j = 0.17 A/cm^2; degradation: 13%/1000 h, T = 950 °C, j = 0.17 A/cm^2; degradation: 26%/1000 h).

3.3. Anode losses R_{1A}, R_{2A}, R_{3A} and $R_{anode\ total}$

The time dependent anode losses R_{1A}, R_{2A} and R_{3A} are shown in Fig. 2(c)–(e), respectively. The resistance R_{1A} can be assigned to the anode gas diffusion losses [5,19]. The absolute value of R_{1A} in gas mixture (2) (H_2–H_2O) at T = 600 °C is much smaller compared to R_{1A} in gas mixture (3) (CO–CO_2) at T = 750 °C and 900 °C. This can be explained by the lower gas diffusion coefficient in CO–CO_2 compared to H_2–H_2O operation leading to a lower R_{1A}-value of cell A even at T = 600 °C. A mostly constant time dependent behavior at each temperature indicates that R_{1A} is not responsible for the degradation behavior of R_{pol} in Fig. 2(a). This holds the same for R_{2A} and R_{3A}. The sum of both RQ elements with the resistances R_{2A} and R_{3A} represents the impedance of the lattice network structure of (i) the Ni/8YSZ anode charge transfer reaction at the triple phase

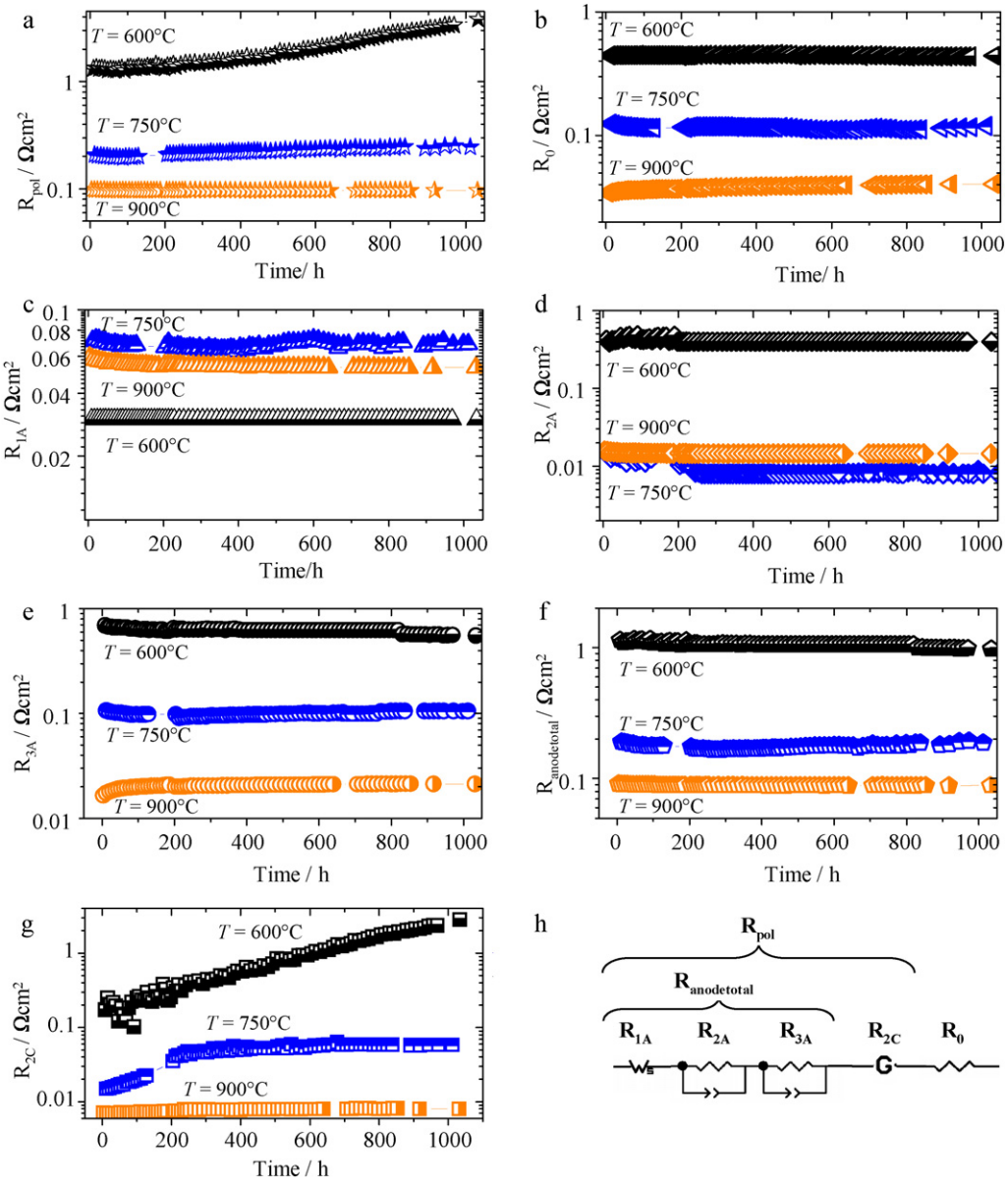

Fig. 2. Time and temperature dependent behavior of (a) the total polarization resistance R_{pol}, (b) the ohmic resistance R_0, (c) R_{1A}, (d) R_{2A}, (e) R_{3A}, (f) $R_{anode\ total}$ and (g) R_{2C}. (h) The equivalent circuit model [5] was applied to identify four individual polarization processes. The resistances at $T = 600\,^{\circ}C$ are determined in anode gas mixture (2) (H_2–H_2O (40/60)), for $T = 750\,^{\circ}C$ and $900\,^{\circ}C$ all contributions are determined in anode gas mixture (3) (CO–CO_2 (50/50)).

Table 2
Total polarization resistances at $t = t_{start}$, $t_{\sim 300\,h}$ and $t = t_{end}$ in gas mixture (2) (H_2–H_2O (40/60)) at the anode for $T = 600\,^{\circ}C$, gas mixture (3) (CO–CO_2 (50/50)) at the anode for $T = 750\,^{\circ}C$ and $900\,^{\circ}C$ and air at the cathode.

Total polarization resistance	R_{pol} at t_{start} [$\Omega\,cm^2$]	R_{pol} at $t_{\sim 300\,h}$ [$\Omega\,cm^2$]	Degradation [%/h]	R_{pol} at t_{end} [$\Omega\,cm^2$]	Degradation [%/h]
R_{pol} Cell A	1.317	1.509	0.049	3.804	0.209
R_{pol} Cell B	0.207	0.214	0.012	0.245	0.02
R_{pol} Cell C	0.0981	0.0969	-4.1×10^{-3}	0.0972	-4.4×10^{-4}

Table 3
Separated cathode polarization resistances at $t = t_{start}$, $t_{\sim 300h}$ and $t = t_{end}$ and calculations of the degradation rate.

Cathode polarization resistance	R_{2C} at t_{start} [$\Omega\,cm^2$]	R_{2C} at $t_{\sim 300\,h}$ [$\Omega\,cm^2$]	Degradation [%/h]	R_{2C} at t_{end} [$\Omega\,cm^2$]	Degradation [%/h]
R_{2C} Cell A	0.173	0.444	0.53	2.823	0.734
R_{2C} Cell B	0.015	0.047	0.72	0.058	0.033
R_{2C} Cell C	0.0071	0.0078	0.031	0.008	0.0036

boundary, (ii) ionic transport in the Ni/8YSZ structure, and (iii) gas diffusion limitation inside the pores of the AFL in approximately the first 100 h of operation [13,14]. R_{2A} shows a constant behavior during the measurement with a slight decrease in the first 200 h. The decrease in R_{2A} can be explained by the change in the Ni/8YSZ structure at the beginning of the measurement. The AFL is a dense layer after initial cell manufacturing. It takes several hours of cell operation until there is a certain open porosity in the structure and the gas diffusion in the AFL can be neglected for each operating temperature. R_{3A} remains constant for $T = 600\,^{\circ}C$ and 750 °C and increases by 30%/1031 h at $T = 900\,^{\circ}C$. So the anode process P_{3A} contributes to the cell degradation at $T = 900\,^{\circ}C$. A well-known anode degradation phenomenon is the Ni agglomeration and the loss of Ni–Ni contact [7,20,21] which reduces the amount of three-phase contacts at the electrolyte/AFL interface and contribute to the increase in anode polarization resistance. However the total polarization resistance R_{pol} remains constant for $T = 900\,^{\circ}C$ so the increase of R_{3A} and also of R_{2C} is obviously compensated by the decreasing contributions R_{1A} and R_{2A}. Considering the total anode polarization resistance $R_{anode\ total}$ in Fig. 2(f) it can be assumed that the accumulated degradation behavior of the anode processes does not affect the time dependent characteristics of R_{pol}.

3.4. Cathode losses R_{2C}

With $pO_2 = 0.21$ atm and an airflow of 250 mL/min the cathodic losses originate from oxygen surface exchange kinetics and from the diffusivity of oxygen ions through the LSCF bulk (R_{2C}) [5,15]. Fig. 2(g) shows the cathode polarization resistance at $T = 600\,^{\circ}C$, 750 °C and 900 °C versus time. The corresponding degradation rates of R_{2C} are shown in Table 3.

At $T = 600\,^{\circ}C$ the cathode polarization resistance increases nonlinear from $0.173\,\Omega\,cm^2$ to $0.444\,\Omega\,cm^2$. This corresponds to a degradation rate of 0.53% ($t = 8$–304 h) and 0.734%/h ($t = 304$–11033 h). A nonlinear increase of R_{2C} was also detected at $T = 750\,^{\circ}C$ with a reversal tendency. R_{2C} increases strongly by 0.72%/h at $t = 11$–304 h and only by 0.033%/h at $t = 304$–1012 h. A saturation effect can be assumed for this temperature from $t = 400$ h regarding Fig. 2(g).

At $T = 900\,^{\circ}C$ a very small but still increasing trend can be observed. A degradation rate of 0.031%/h ($t = 3$–1319 h) and 0.0036%/h ($t = 319$–11031 h) was determined. It can be concluded that the degradation rates of the cathode losses R_{2C} show an increasing trend with decreasing temperature comparable with the time related behavior of R_{pol}.

These results indicate that the degradation behaviour of the cathode is responsible for the degradation of the polarization resistance R_{pol} especially at $T = 600\,^{\circ}C$ and 750 °C. There are hardly systematically investigations in literature about the time and temperature dependent behavior of the cathode polarization resistance. But different explanations are given as potential causes of the cathode degradation:

- Mai and Becker [1,3,4] analyzed the same type of LSCF cathodes (identical composition and sintering procedure) on ASCs after long term measurements ($t = 1000$ h) by secondary ion mass spectroscopy (SIMS) and found an enrichment of Sr on the CGO/YSZ electrolyte surface deposited in gas flow direction. This finding corresponds to a depletion of Sr in the cathode bulk or at the cathode surface.
- The same type of LSCF cathodes on ASCs, but with electron-beam evaporated (EB-PVD) CGO were analyzed recently by TEM measurements. A slight enrichment of Gd in the LSCF cathode already after the sintering procedure was found [22].
- LSC thin films ($La_{0.6}Sr_{0.4}CoO_3$ with a thickness of 100 nm) on YSZ substrates were investigated by Dieterle [23]. Sr depletion and the formation of Co-rich phases were confirmed already after an exposure time of 8 h at 700 °C.
- Xiong [24] suggests sulfur poisoning in the cathode air as degradation cause. $(La_{0.85}Sr_{0.15})_{0.95}MnO_3$ and $Sm_{0.5}Sr_{0.5}CoO_3$ cathodes on $La_{0.8}Sr_{0.2}Ga_{0.8}Mg_{0.15}Co_{0.05}O_3$ electrolytes with Pt counter electrode were investigated at $T = 800\,^{\circ}C$ under SO_2-air mixture. The high activity of SrO in cobaltite-based cathodes causes the formation of $SrSO_4$ in SO_2-concentrated air. After a reaction with SO_2 CoO is formed as one of the decomposition products of the SrSmCo phase.

These results indicate an instability of the chemical composition of mixed ionic–electronic conducting cathodes like LSCF (or LSC) at relatively low temperatures and for short operation times. Instability on the A-site of the perovskite type compound is well known for electronic conducting cathodes like LSM ((La, Sr)MnO_3), which react with the electrolyte YSZ to $SrZrO_3$ or to a pyrochlore phase of the composition $LaZr_2O_7$ [25]. To explain the temperature dependent degradation behaviour of the LSCF cathode found in this study we assume that the degradation mechanism is not a temperature driven demixing or decomposition process. The compositional and/or structural changes should be analyzed with the following methods: (a) TEM and SAED analysis of individual grains of the LSCF cathode structure before and after the long term measurement. Moreover, the selection of different volume areas in the LSCF cathode is indispensable to satisfy statistics. (b) Wet-chemical analysis of the LSCF "as manufactured" and after the long term measurements can also discover possible changes in composition. However, this method defines the stoichiometry with an accuracy about 3–20% depending on the amount of material analyzed. (c) XRD measurements followed by the determination of the lattice parameters can reveal compositional/structural changes before and after the measurements. (d) Energy-dispersive X-ray spectrometry (EDXS) measurements on cross-section samples of the LSCF cathode may prove changes in composition before and after the long term measurement.

4. Conclusions

Knowledge about the contributions of anodic and cathodic polarization losses and their time and temperature dependence is essential for the profound development of ASCs. For the first time cathodic and anodic polarization losses of state-of-the-art ASCs were separated by selective experimental parameters and high resolution impedance studies. EIS data were monitored in long term measurements at $T = 600\,^{\circ}C$, 750 °C and 900 °C over 1000 h of operation and interpreted on the basis of a physically reasonable equivalent circuit model by (i) a DRT analysis followed by (ii) a CNLS fit. As a result, the following conclusions can be stated:

(i) R_{pol}: The total polarization resistance R_{pol} shows a time and temperature dependent behaviour. The degradation rates increase with decreasing temperature. By using the method of distribution of relaxation times (DRT) combined with a complex nonlinear least square (CNLS) fitting approach the total polarization resistance can be separated in three anode resistances R_{1A}, R_{2A} and R_{3A} and a cathode resistance R_{2C}.

(ii) R_{1A}, R_{2A}, R_{3A} and $R_{anode\ total}$: The single anode contributions show a temperature and time dependent behavior. While R_{1A} remains constant, R_{2A} is decreasing slightly in the first 200 h. Only R_{3A} is increasing by 30% at $T = 900\,^{\circ}C$ indicating the degradation of the anode material. Considering the sum of all anode contributions $R_{anode\ total}$ remains constant for all temperatures and does not contribute to the degradation of the polarization resistance R_{pol}.

(iii) R_{2C}: The LSCF cathode resistance R_{2C} is initially very small and causes only 12–15% of the total polarization resistance depending on the operating temperature. But R_{2C} increases during the measurement by 1.49%/h at $T = 600\,^{\circ}C$, 0.28%/h at $T = 750\,^{\circ}C$ and 0.012%/h at $T = 900\,^{\circ}C$. The degradation of R_{2C} increases with decreasing temperature which is an essential result for the further development of ASC with LSCF cathode in intermediate temperature operating conditions.

This study gives evidence that the time dependent cathode loss of a state-of-the-art ASC for IT-SOFC is essentially influenced by the operating temperature, if a MIEC material like $La_{0.58}Sr_{0.4}Co_{0.2}Fe_{0.8}O_{3-\delta}$ is chosen. The reason of the degradation is likely due to the Sr (and Co) depletion, as reported earlier [1,3,4,22,23] and sulphur poisoning [24] but these suggestions do not explain the temperature dependence gained in this study in detail. A more precise analysis of the largest cathode degradation mechanism especially at $T = 600\,^{\circ}C$ is still necessary. Finally, it should be pointed out that for the investigated ASC at $T = 750\,^{\circ}C$ and $T = 900\,^{\circ}C$ the anode is responsible for the largest part of the polarization losses.

References

[1] M. Becker, Parameterstudie zur Langzeitstabilität von Hochtemperaturbrennstoffzellen (SOFC), Ph.D. Thesis, Universität Karlsruhe (TH), Germany (2007).

[2] L.G.J. de Haart, I.C. Vinke, A. Janke, H. Ringel, F. Tietz, Solid oxide fuel cells VII (SOFC-VII), in: H. Yokokawa, S.C. Singhal (Eds.), PV 2001-16, The Electrochemical Society Proceedings, Pennington, NJ, 2001, pp. 111–119.

[3] A. Mai, M. Becker, W. Assenmacher, F. Tietz, D. Hathiramani, E. Ivers-Tiffée, D. Stöver, W. Mader, Time-dependent performance of mixed-conducting SOFC cathodes, Solid State Ionics 177 (2006) 1965.

[4] A. Mai, V.A.C. Haanappel, S. Uhlenbruck, F. Tietz, D. Stöver, Ferrite-based perovskites as cathode materials for anode-supported solid oxide fuel cells, Solid State Ionics 176 (2005) 1341.

[5] A. Leonide, V. Sonn, A. Weber, E. Ivers-Tiffée, Evaluation and modelling of the cell resistance in anode-supported solid oxide fuel cells, J. Electrochem. Soc. 155 (2008) B36.

[6] C. Endler, A. Leonide, A. Weber, F. Tietz, E. Ivers-Tiffée, Time-dependent electrode performance changes in intermediate temperature solid oxide fuel cells, J. Electrochem. Soc. 157 (2) (2010) B292.

[7] A. Hagen, R. Barfod, P.V. Hendriksen, Y.L. Liu, S. Ramousse, Degradation of anode supported SOFCs as a function of temperature and current load, J. Electrochem. Soc. 153 (2006) A1165.

[8] H.P. Buchkremer, U. Diekmann, D. Stöver, Components manufacturing and stack integration of an anode supported planar SOFC system, in: B. Thorstensen (Ed.), Proceedings of the 2nd European Solid Oxide Fuel Cell Forum, European Fuel Cell Forum, Oberrohrdorf, Switzerland, 1996, p. 221.

[9] F. Tietz, A. Mai, D. Stöver, From powder properties to fuel cell performance—a holistic approach for SOFC cathode development, Solid State Ionics 179 (2008) 1509–1515.

[10] A. Weber, A. Müller, D. Herbstritt, E. Ivers-Tiffée, Characterization of SOFC single cells, in solid oxide fuel cells VII, in: H. Yokokawa, S.C. Singhal (Eds.), The Electrochemical Society Proceedings Series, Pennington NJ, 2001.

[11] D. Johnson, ZPlot, ZView Electrochemical Impedance Software, Version 2.3b, Scribner Associates, Inc., 2000.

[12] H. Schichlein, A. Müller, M. Voigts, A. Krügel, E. Iver-Tiffée, Deconvolution of electrochemical impedance spectra for the identification of electrode reaction mechanisms in solid oxide fuel cells, J. Appl. Electrochem. 32 (2002) 875.

[13] V. Sonn, A. Leonide, E. Ivers-Tiffée, Combined deconvolution and CNLS fitting approach applied on the impedance response of technical Ni/8YSZ cermet electrodes, J. Electrochem. Soc. 155 (2008) B675.

[14] A. Leonide, S. Ngo Dinh, A. Weber, E. Ivers-Tiffée, Performance limiting factors in anode supported SOFC, in: R. Steinberger-Wilckens, U. Bossel (Eds.), Proceedings of the 8th European Solid Oxide Fuel Cell Forum, 2008, p. A0501.

[15] S.B. Adler, J.A. Lane, B.C.H. Steele, Electrode kinetics of porous mixed-conducting oxygen electrodes, J. Electrochem. Soc. 143 (1996) 3554.

[16] L.W. Tai, M.M. Nasrallah, H.U. Anderson, D.M. Sparlin, S.R. Sehlin, Structure and electrical-properties of $La_{1-X}Sr_xCo_{1-Y}Fe_yO_3$: 1. The system $La_{0.8}Sr_{0.2}Co_{1-Y}Fe_yO_3$, Solid State Ionics 76 (1995) 259–271.

[17] A.C. Müller, Mehrschicht-Anode für die Hochtemperatur-Brennstoffzelle (SOFC), Ph.D. Thesis, Universität Karlsruhe (TH), Germany (2004).

[18] O. Yamamoto, Solid oxide fuel cells: fundamental aspects and prospects, Electrochim. Acta 45 (2000) 2423–2435.

[19] S. Primdahl, M. Mogensen, Gas diffusion impedance in characterization of solid oxide fuel cell anodes, J. Electrochem. Soc. 146 (1999) B8.

[20] D. Simwonis, F. Tietz, D. Stöver, Nickel coarsening in annealed Ni/8YSZ anode substrates for solid oxide fuel cells, Solid State Ionics 132 (2000) 241.

[21] D. Fouquet, A. Müller, A. Weber, E. Ivers-Tiffée, Kinetics of oxidation and reduction of Ni/YSZ cermets, in: J. Huijsmans (Ed.), Proceedings of the Fifth European Solid Oxide Fuel Cell Forum, European Fuel Cell Forum, Oberrohrdorf, Switzerland, 2002, p. 467.

[22] S. Uhlenbruck, T. Moskalewicz, N. Jordan, H.-J. Penkalla, H.P. Buchkremer, Element interdiffusion at electrolyte–cathode interfaces in ceramic high-temperature fuel cells, Solid State Ionics 180 (2009) 418.

[23] L. Dieterle, D. Bach, R. Schneider, H. Störmer, D. Gerthsen, U. Guntow, E. Ivers-Tiffée, A. Weber, C. Peters, H. Yokokawa, Structural and chemical properties of nanocrystalline $La_{0.5}Sr_{0.5}CoO_{3-\delta}$ layers on yttria-stabilized zirconia analyzed by transmission electron microscopy, J. Mater. Sci. 43 (2008) 3135.

[24] Y. Xiong, K. Yamaji, T. Horita, H. Yokokawa, J. Akikusa, H. Eto, T. Inagaki, Sulfur poisoning of SOFC cathodes, J. Electrochem. Soc. 156 (5) (2009) B588.

[25] A. Weber, R. Männer, R. Waser, E. Ivers-Tiffée, Interaction between microstructure and electrical properties of screen printed cathodes in SOFC single cells, Denki Kagaku J. Electrochem. Soc. Jpn. 64 (6) (1996) 582.